



Bimetallic Co–Ni/TiO₂ catalysts for selective hydrogenation of cinnamaldehyde

Saranya Ashokkumar, et al. [full author details at the end of the article]

Received: 7 March 2018 / Accepted: 18 June 2018
© Springer Nature B.V. 2018

Abstract

Bimetallic Co–Ni catalysts in the composition range Co_(1-x)Ni_x with $x = 0.0, 0.2, 0.3, 0.4, 0.5, 0.6, 0.8$ and 1.0 , with total metal loading of 15% w/w and supported on TiO₂-P25, have been prepared by chemical reduction of the metal acetates by glucose in aqueous alkaline medium and characterized by XRD, TEM, TPR, XPS and H₂-TPD techniques. Selective hydrogenation of cinnamaldehyde (CAL) to hydrocinnamaldehyde (HCAL), cinnamyl alcohol (COL) and hydrocinnamyl alcohol (HCOL) has been investigated at 20 bar pressure, in the temperature range 120–140 °C. Co/Ni crystallite sizes in the range 6.0 ± 1 nm are observed by TEM. TPR and XPS results indicate the formation of nanoscale Co–Ni alloys, which tend to weaken M–H bond strength, as revealed by H₂-TPD measurements. Ni/TiO₂ displays very high conversion of CAL (86.9%) with high selectivity (78.7%) towards HCAL formation at 140 °C. Co/TiO₂, on the other hand, exhibits relatively lower CAL conversion (55%) and higher selectivity (61.3%) for COL formation at the same temperature. However, bi-metallic Co–Ni catalysts in the composition range $x = 0.3–0.6$ display very high conversion (> 98%) due to alloy formation and weakening of M–H bonds. Bimetallic Co_{0.7}Ni_{0.3} catalyst displays high conversion of CAL (98.1%) and high selectivity (82.9%) towards HCOL. Overall CAL hydrogenation activity at 140 °C, when expressed as TOF, displays a maximum value at the composition Co_{0.5}Ni_{0.5}. Activity and selectivity patterns have been rationalized based on the reaction pathways observed on the catalysts and the influence of Co–Ni alloy formation and M–H bond strength. Thus, a synergetic effect, originating from an appropriate composition of base metal catalysts and reaction conditions, could result in hydrogenation activity comparable with noble metal based catalysts.

Keywords Co–Ni bimetallic catalysts · Titania · Co–Ni alloys · Cinnamaldehyde hydrogenation · Metal-hydrogen bond strength

Electronic supplementary material The online version of this article (<https://doi.org/10.1007/s11164-018-3517-7>) contains supplementary material, which is available to authorized users.

Introduction

Selective hydrogenation of cinnamaldehyde (CAL) to cinnamyl alcohol (COL) and hydro-cinnamaldehyde (HCAL) is an important reaction from industrial as well as academic points of view [1,2]. Bimetallic catalysts, in general, display high activity and selectivity for this reaction [3]. Noble metal (Pt and Ru) based bimetallic catalysts with promoters like Co, Sn exhibit high activity and selectivity for COL [4–7]. Non-noble metal based bimetallic catalysts containing Co, Ni and Cu have also been studied extensively [8–12]. Considering the higher cost of noble metal based catalysts, attempts are being made to develop bimetallic catalysts based on Ni and Co [13–15]. Earlier work in this direction by Reddy et al. [13] on 10% Co-10% Ni supported on SiO₂ for vapor phase hydrogenation of CAL resulted in 63% conversion, with 59% selectivity to HCAL and 34% to HCOL and no COL formation. Hui et al. [14] in their studies on unsupported tri-component alloys with varying Co, Ni and B contents as catalysts, have reported maximum CAL conversion of 64.6% for Ni_{38.1}Co_{26.3}B_{35.6} catalyst with nearly total selectivity to HCAL and again no COL. Malobela et al. [15] have observed that bimetallic Co–Ni catalysts of specific composition (5 w/w % each of Ni and Co) on MWCNT support displays 63% CAL conversion with 62% selectivity towards COL.

While titania supported Ni catalyst [16] displays high activity for CAL conversion with high selectivity for HCAL, the corresponding cobalt catalyst displays lower conversion and good selectivity for COL [17]. Bimetallic catalysts with optimum Co–Ni composition could lead to higher activity and selectivity, and this aspect has not been explored so far. A systematic study involving the whole range of Co–Ni composition is needed to arrive at the optimum one. Accordingly, mono and bi-metallic Co–Ni catalysts in the composition range Co_(1-x)Ni_x with $x = 0.0, 0.2, 0.3, 0.4, 0.5, 0.6, 0.8$ and 1.0, supported on TiO₂-P25, have been explored to arrive at the compositions that would give high CAL conversions, comparable to that of noble metal catalysts and good selectivity for COL.

Experimental

Materials

TiO₂-P-25 (Evonik), Ni(CH₃COO)₂·4H₂O (CDH), Co(CH₃COO)₂·4 H₂O (CDH), D-glucose (Merck), methanol, liquor ammonia (Qualigens) and Cinnamaldehyde (Aldrich) were used as such.

Preparation of mono metallic catalysts

The 0.743 g cobalt acetate or 0.746 g of nickel acetate and 40 ml of aqueous D-glucose solution (0.15 M) were mixed and stirred for 30 min at room temperature. Then 10 ml of liquor ammonia was added drop-wise to the mixture. On refluxing the mixture for 5 h at 80 °C, its color turned to black, indicating reduction of Co²⁺/Ni²⁺ ions to Co⁰/Ni⁰. As known, D-glucose acts as reducing as well as capping agent

[18]. Reduction of Co²⁺ and Ni²⁺ ions to their respective metallic state was confirmed by UV–Vis spectroscopic study (Fig. S1), which showed the absence of absorption maxima due to the respective metal ions [19, 20]. Ni/Co nanoparticles, stabilized in alkaline medium, were then anchored on to the support by adding 1 g of TiO₂ (P25) and stirring continued for 2 h. The mixture was cooled to ambient temperature, centrifuged, washed with anhydrous ethanol and dried at 60 °C for 24 h. The catalysts were then pre-reduced in hydrogen gas flow at 300 °C for 3 h, prior to all characterization and hydrogenation experiments.

Preparation of Co–Ni bimetallic catalysts

Co_{1–x}Ni_x bimetallic catalysts with different atomic fractions with $x = 0.0, 0.2, 0.3, 0.4, 0.5, 0.6, 0.8$ and 1.0 were prepared using the same green chemistry route followed for monometallic catalysts. In all the bimetallic catalysts total metal loading (Co + Ni) was maintained at 15% w/w. Appropriate quantities of Co and Ni acetates, as defined by the value of x , were mixed in aqueous glucose solution and subjected to simultaneous chemical reduction, which was confirmed by UV–visible spectroscopy (Fig. S1). After washing the final catalysts with ethanol and drying at 60 °C, the catalysts were pre-reduced in hydrogen gas flow at 300 °C for 3 h. All characterization and hydrogenation experiments were carried out with pre-reduced catalysts.

Characterization of catalysts

Co and Ni contents in the catalysts were estimated by the ICP-OES technique, using a Perkin Elmer Model Optima 5300 DV unit, after extraction of the metals with aqua regia.

Powder X-Ray diffraction patterns for the catalysts were recorded by using a Rigaku Miniflex II X-ray diffractometer with Cu-K α ($\lambda = 0.15418$ nm) radiation in the 2θ range of 10°–80° and at a scan rate of 3°/min.

Temperature programmed reduction (H₂-TPR) and temperature programmed desorption (H₂-TPD) runs were carried out using a Micromeritics Autochem II 2920 chemisorption analyser. For TPR, the catalysts were pre-calcined in air at 300 °C for 3 h. Then 50 mg of calcined catalyst was pre-treated at 300 °C in high purity Ar gas (25 cc/min) for 1 h and then cooled to room temperature in an Ar flow. The gas was changed to 10% H₂ in Ar (25 cc/min) at room temperature. After the stabilization of the baseline, TPR was started from RT to 700 °C with a heating rate 10 °C/min.

For H₂ TPD measurements, 50 mg of catalyst was reduced in hydrogen flow (25 cc/min) at 300 °C for 4 h and cooled to ambient temperature. Ar flow (30 cc/min) was then introduced, and the catalyst was purged for 30 min. After the stabilization of the baseline, TPD of H₂ was recorded up to 700 °C at a temperature ramp of 10 °C/min.

Transmission electron micrographs were recorded using a JEOL 3010 model microscope. Few milligrams of the reduced samples (1–2 mg) were dispersed in a few mL (1–2 mL) of ethanol by ultra-sonication for 15 min and a drop of the

dispersion was placed on a carbon coated copper grid and allowed to dry in air at room temperature.

Based on the mean crystallite size measured from TEM data, Co/Ni metal dispersion were calculated using the formula [21]

$$\text{Dispersion (\%)} = \frac{600 \times M_{\text{Co/Ni}}}{\rho_{\text{Co/Ni}} \times d_{\text{nm}} \times a_{\text{Co/Ni}} \times N_{\text{a}}}, \quad (1)$$

where M is the molecular weight of the metal (Co/Ni), a is the atomic surface area of Co/Ni ($6.62/6.49 \times 10^{-20} \text{ m}^2/\text{atom}$), $\rho_{\text{Co/Ni}}$ is the density of the metals, N_{a} is Avogadro's number, and d_{nm} is the average crystallite diameter (in nm) estimated from TEM data.

XPS spectra of the catalysts were recorded using an Omicron ESCA Probe spectrometer with Mg K_{α} X-rays ($h\nu = 1253.6 \text{ eV}$). The samples were spotted as drop cast films on a sample stub. The base pressure of the analysis chamber during the scan was 2×10^{-10} millibar. The pass energies for individual and survey scans were 20 and 100 eV, respectively. The spectra were recorded with a step width of 0.05 eV. Data were processed with the Casa XPS program (Casa Software Ltd.UK), and calibrated with reference to the adventitious carbon peak (284.9 eV) of the sample.

Hydrogenation of cinnamaldehyde

Catalysts were evaluated for liquid phase hydrogenation of cinnamaldehyde (CAL) in a 100 mL Parr reactor (Model-4848). Initially, the reactor was filled 15 g of iso-propanol and 1.65 g of water as solvent. Use of this mixture as solvent [7] resulted in very little formation of acetals during hydrogenation. Also, 1.2 g of CAL and 150 mg of catalyst were then added to the solvent mixture. The reactor was purged three times with H_2 gas and then pressurized to 20 bar. Normally the reaction was carried out for 1 h in the temperature range 120–140 °C. A 1 h time is noted from the moment the reactor reaches the specified temperature. After each reaction, the reactor is allowed to cool naturally to room temperature, catalyst and reaction products were separated by filtration, and the product stream was analyzed in a Perkin Elmer Clarus-500 GC equipped with a ZB-1 capillary column and FID.

Calculation of conversion The reaction mixture containing (15 g iso-propanol + 1.65 g water and 1.2 g CAL) was used as standard, representing the initial concentration of CAL. Analysis of this mixture was carried out before every reaction run. Then 0.4 μL standard is injected into GC and its area is noted. 0.4 μL of reaction products is then analyzed, and the conversion is calculated as follows:

$$\% \text{ Conversion} = \frac{A_{\text{S}} - A_{\text{RP}}}{A_{\text{S}}} \times 100. \quad (2)$$

A_{S} —Area of CAL in standard mixture, A_{RP} —Area of CAL in reaction product

$$\% \text{ Selectivity} = \frac{A_{SP}}{\sum \text{Products}} \times 100 \quad (3)$$

A_{SP} —Area of product whose selectivity to be calculated, $\sum \text{Products}$ —sum of areas of all products

Rates of hydrogenation (r) and Co/Ni metal dispersion (calculated using formula-1) values were utilized to compute Turn over Frequency (TOF) using the formula-2 [21]

$$\text{TOF} = \frac{r}{n_{\text{tot}} \times \text{Dispersion}(\%)}, \quad (4)$$

where r is the rate of hydrogenation (moles converted per second), n_{tot} is the total number of Co/Ni moles in the reactor.

Results and discussion

Chemical composition

Actual chemical composition of the catalysts, in terms Co and Ni contents, as analyzed by ICP-AES technique, are given in Table S1. Actual values are close to the expected values, thus confirming the chemical composition of the catalysts.

X-ray diffraction

XRD patterns for monometallic Co and Ni catalysts and six different bimetallic catalyst formulations are given in Fig. 1. According to JCPDS data, metallic Ni exhibits major d-lines, at $2\theta = 44.505^\circ$, 51.84° and 76.37° (04-0850) and metallic Co at $2\theta = 44.227^\circ$, 51.53° and 75.865° (89-7093). X-ray diffractogram for Ni/TiO₂ displayed characteristic d-lines due to support TiO₂-P-25 and in addition, only one d-line at 44.38° due to metallic Ni. The other two lines at $2\theta = 51.84^\circ$ and 76.37° are not observed due to the weak intensity. Likewise, in the case of Co/TiO₂, besides the d-lines due to TiO₂-P-25 phase, an extra d-line at $2\theta = 44.18^\circ$ attributed to metallic Co is noticed. Additional d-lines at $2\theta = 51.53^\circ$ and 75.865° are not observed. Both monometallic catalysts prepared in this work exhibit fcc crystal structure.

All the six bimetallic Co–Ni catalysts exhibit d-lines in the range $2\theta = 44.1$ – 44.3° , which is within the 2θ values of 44.18° and 44.38° observed in this work for Co and Ni metals, respectively. Such shifts in the d-lines in the case of titania supported Ni–Co bimetallic catalysts was observed by Takanaabe et al. [22] and attributed to alloy formation. The 2θ values in the range 44.1 – 44.3° observed for bimetallic catalysts are also close to the major d-line at $2\theta = 44.48^\circ$, reported for Ni–Co alloys (071-074-5694). Since the crystallite sizes are small, the d-lines are broader, but the formation of alloys is imminent. Malobela et al. [15] in their studies on 5% Ni–5% Co catalysts on carbonaceous supports, (graphite, MWCNT and activated carbon) have also observed the formation of Ni₅₀Co₅₀ alloy.

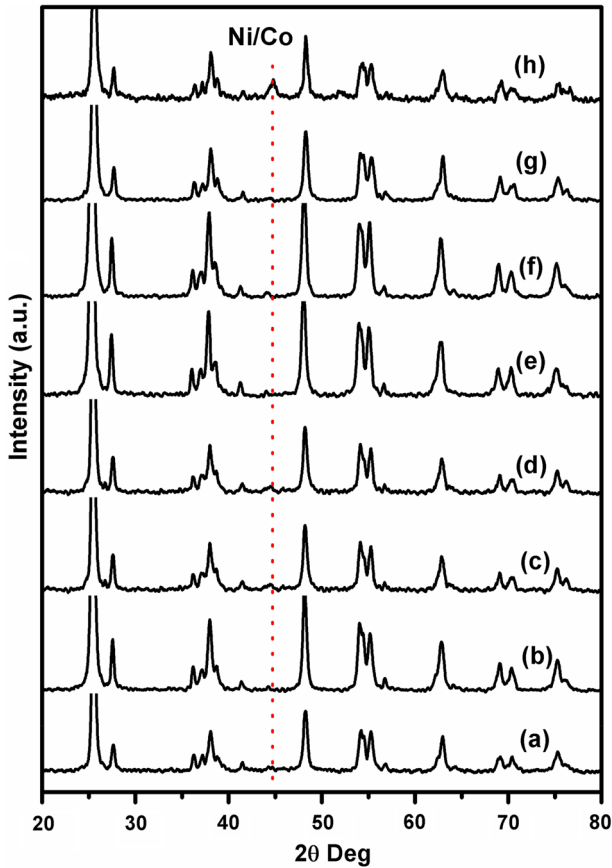


Fig. 1 X-ray diffractograms for *a* Co/TiO₂ *b* Co_{0.8} Ni_{0.2}/TiO₂ *c* Co_{0.7} Ni_{0.3}/TiO₂ *d* Co_{0.6} Ni_{0.4}/TiO₂ *e* Co_{0.5} Ni_{0.5}/TiO₂ *f* Co_{0.4} Ni_{0.6}/TiO₂ *g* Co_{0.2} Ni_{0.8}/TiO₂ *h* Ni₁/TiO₂

No d-lines due to Co with hcp structure are observed, though Co rich catalysts may contain unalloyed Co phase [23]. According to Zhang et al. [24], hcp phase may appear when Co crystallite size is larger than 17 nm. In the present work, since crystallite size of Co is < 17 nm, only fcc structure is favored. Crystallite size values calculated using the Debye–Scherrer equation, are in the range of 5–11 nm (Table 1). However, when prepared in unsupported form, Co nanoparticles with hcp as well as fcc structure are observed, while in presence of titania support, only the fcc phase is observed.

Transmission electron microscopy

Figure 2 presents transmission electron micrographs along with histograms for all eight catalyst samples. Finely dispersed Co/Ni crystallites in the size range 6 ± 1.0 nm could be observed clearly on the titania support. While monometallic Co or Ni catalyst displays crystallites of mean size 6.5 and 6.9 nm, respectively, in

Table 1 Crystallite size and TOF values for Co–Ni catalysts

Catalysts	Cryst. size ^a (nm)	Cryst. size ^b (nm)	TOF × 10 ⁻¹ (h ⁻¹) ^c
Co ₁	8.0	6.5	1.08
Co _{0.8} Ni _{0.2}	5.6	5.5	1.44
Co _{0.7} Ni _{0.3}	5.5	5.1	1.54
Co _{0.6} Ni _{0.4}	8.1	7.0	1.58
Co _{0.5} Ni _{0.5}	11.0	6.4	1.80
Co _{0.4} Ni _{0.6}	7.4	5.0	1.44
Co _{0.2} Ni _{0.8}	6.2	6.1	1.51
Ni ₁	10.0	6.9	1.69

^aXRD, ^bTEM, ^cat 140 °C

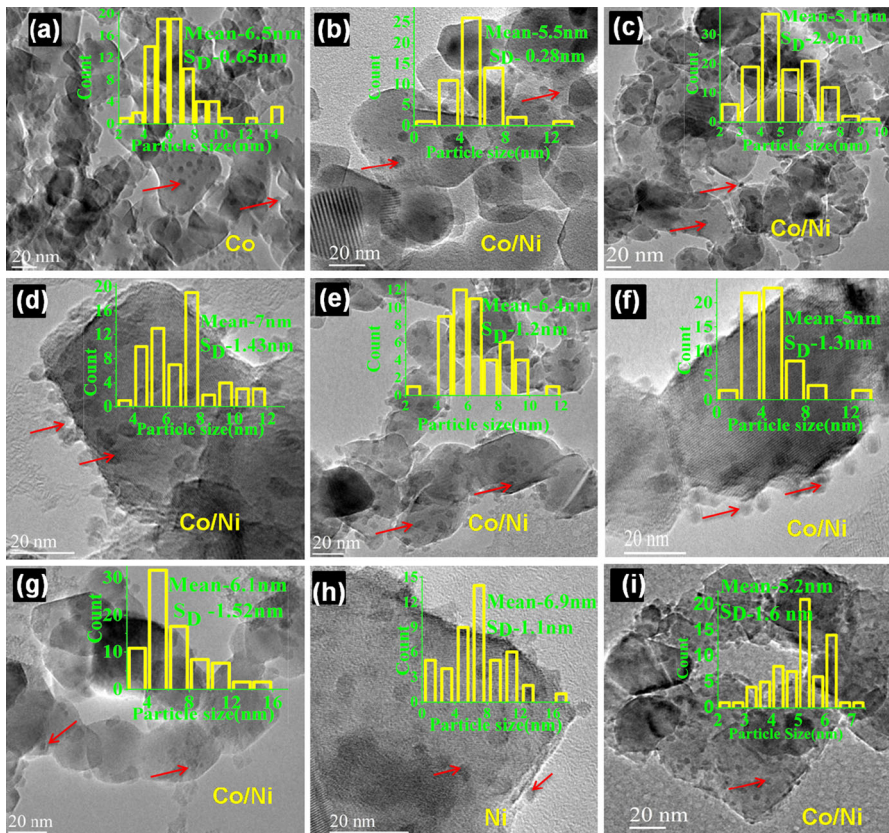


Fig. 2 TEM micrographs with histograms for **a** Co/TiO₂ **b** Co_{0.8} Ni_{0.2}/TiO₂ **c** Co_{0.7} Ni_{0.3}/TiO₂ **d** Co_{0.6} Ni_{0.4}/TiO₂ **e** Co_{0.5} Ni_{0.5}/TiO₂ **f** Co_{0.4} Ni_{0.6}/TiO₂ **g** Co_{0.2} Ni_{0.8}/TiO₂ **h** Ni/TiO₂ **i** Co_{0.7} Ni_{0.3}/TiO₂ (Used)

Co–Ni bi-metallic catalysts, a relatively smaller size range, 5.0 to 5.5 nm crystallites are observed. Crystallite size values obtained by TEM and XRD are comparable (Table 1).

Temperature programmed reduction

TPR profiles for mono- and bimetallic catalysts are presented in Fig. 3. For better clarity, as recorded TPR profiles for individual catalysts are given in Fig. S2. Monometallic Ni/TiO₂ shows major reduction maximum at 387 °C, attributed to the reduction of Ni²⁺ ions that have interacted with the support (Profile-h). Reduction of dispersed Ni²⁺ ions is indicated at 230 and 300 °C, as shoulders to the major peak. Continuation of reduction beyond 450 °C is due to the reduction of Ni²⁺ ions with strong interaction with the support. Reduction of dispersed Co²⁺ ions (Profile-a) is indicated in the form of shoulders at 250 °C and a peak at 333 °C, followed by another peak at 380 °C due to Co²⁺ ions that have interacted with the support. Reduction maximum at 488 °C is due to Co²⁺ with relatively stronger interaction

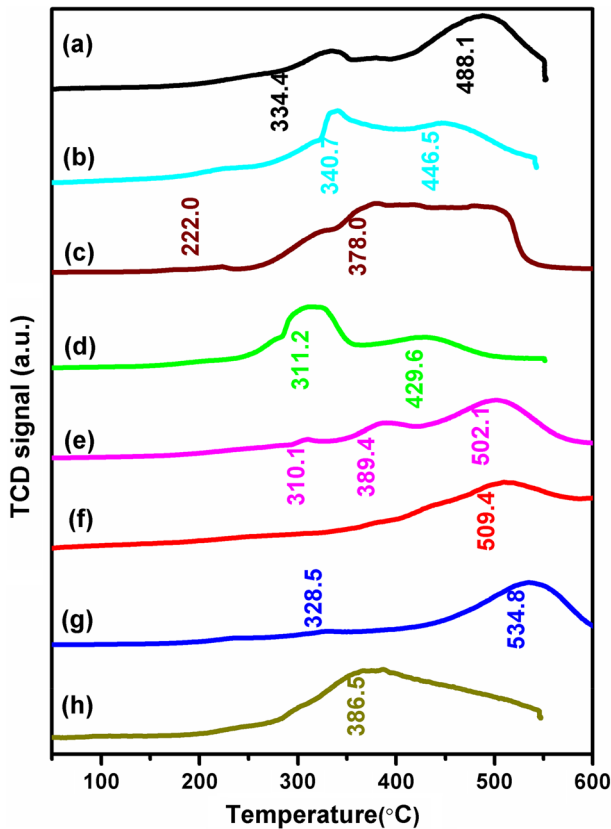


Fig. 3 H₂-TPR Profiles for *a* Co/TiO₂ *b* Co_{0.8} Ni_{0.2}/TiO₂ *c* Co_{0.7} Ni_{0.3}/TiO₂ *d* Co_{0.6} Ni_{0.4}/TiO₂ *e* Co_{0.5} Ni_{0.5}/TiO₂ *f* Co_{0.4} Ni_{0.6}/TiO₂ *g* Co_{0.2} Ni_{0.8}/TiO₂ *h* Ni₁/TiO₂

with the support. Addition of Ni to the extent of 0.2 atom fraction (Co_{0.8}Ni_{0.2}, profile-b), results in shifting of the reduction processes to lower temperatures. Dispersed Ni²⁺ and Co²⁺ ions get reduced at 230, 330 °C, and the reduction peaks at 387 and 380 °C, observed for mono metallic Ni²⁺ and Co²⁺ respectively, merge at 341 °C, possibly due to simultaneous reduction and/or alloy formation. Besides, the high temperature reduction peak 488 °C due to Co²⁺ is shifted to 447 °C, indicating weaker Co-support interaction. Since Ni²⁺ ions undergo reduction ($E_{\text{Ni(II)/Ni}} = -0.250$ V vs. SHE) prior to Co²⁺ ions ($E_{\text{Co(II)/Co}} = -0.277$ V vs. SHE) [25], Ni metal crystallites catalyze the reduction of Co²⁺ with the nascent hydrogen formed on the Ni surface, and; hence, the alloy formation and Co²⁺ reduction at lower temperature (488–447 °C) is facilitated. Further addition of Ni to Co_{0.7}Ni_{0.3} (profile-c) increases overall reducibility, with the Ni metal catalyzing the reduction of Co²⁺ ions. Due to facile reduction, the peaks at 330, 378, 420 and 480 °C merge, indicating simultaneous Ni²⁺ and Co²⁺ reduction and alloy formation. Bimetallic catalyst composition Co_{0.6}Ni_{0.4} (profile-d) with higher Ni content presents a distinct peak at 311 °C due to Co²⁺ and Ni²⁺ reduction and alloy formation along with a shoulder at 280 °C and another peak due to supported Co²⁺ getting reduced at lower temperature, i.e., 430 °C. With the composition Co_{0.5}Ni_{0.5} (profile-e), besides the peak at 390 °C due to Co–Ni alloy, and high temperature reduction peak at 505 °C, is observed. With further increase in Ni content (Co_{0.4}Ni_{0.6}) alloy content decreases and its reduction peak merges (profile-f) with that due to reduction of Ni²⁺ at 510 °C, due to strong interaction with the support. TPR profile-g for bi-metallic composition Co_{0.2}Ni_{0.8} shows very little alloy formation and a major reduction peak at 535 °C that is due to Ni²⁺ strongly bound to the support.

To summarize, TPR profiles indicate maximum Co–Ni alloy formation and high reducibility in the composition range Co_{0.7}Ni_{0.3}–Co_{0.5}Ni_{0.5} and minimum/weaker interaction with the support. Outside this composition range, interaction of Co/Ni with the support is prominent. Co–Ni alloy formation and increase in reducibility could influence the activation of the reactants and the nature of adsorbed hydrogen, which, in turn affect the activity.

Alloy formation in Co–Ni bimetallic systems and its influence on the activity for various reactions has been reported earlier for other reactions like, steam methane reforming [26], dry reforming of methane with CO₂ [22, 27], steam reforming of alcohols [28] and acetic acid [29], hydrogenation of CO [30–32], methane partial oxidation [33], hydrogenation of furfural [34] and hydrogenation of benzaldehyde [35]. In such reactions, Ni–Co alloys suppress coke formation and retard deactivation, possibly by hydrogenation of coke precursors. Temperature programmed surface hydrogenation studies [36] support such a mechanism, which essentially involves generation of active hydrogen for hydrogenation of coke precursors.

XPS analysis

Figures 4 and 5 present XPS profiles for Co2p_{3/2} and Ni2p_{3/2} energy levels, respectively, for selected Co–Ni bimetallic and monometallic Co and Ni catalysts. Binding energy (BE) values observed for these catalysts are tabulated in Table 2.

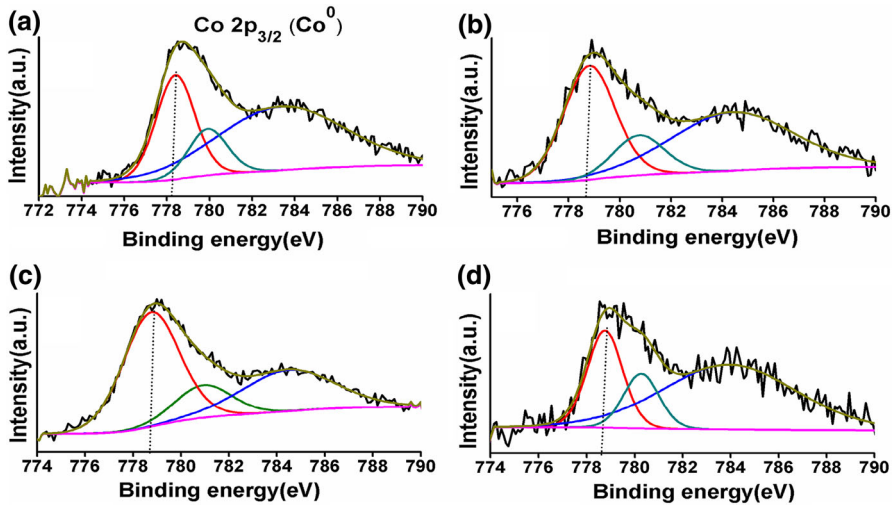


Fig. 4 XPS Profiles for Co2p level a Co/TiO₂ b Co_{0.7} Ni_{0.3}/TiO₂ c Co_{0.6} Ni_{0.4}/TiO₂ d Co_{0.5} Ni_{0.5}/TiO₂

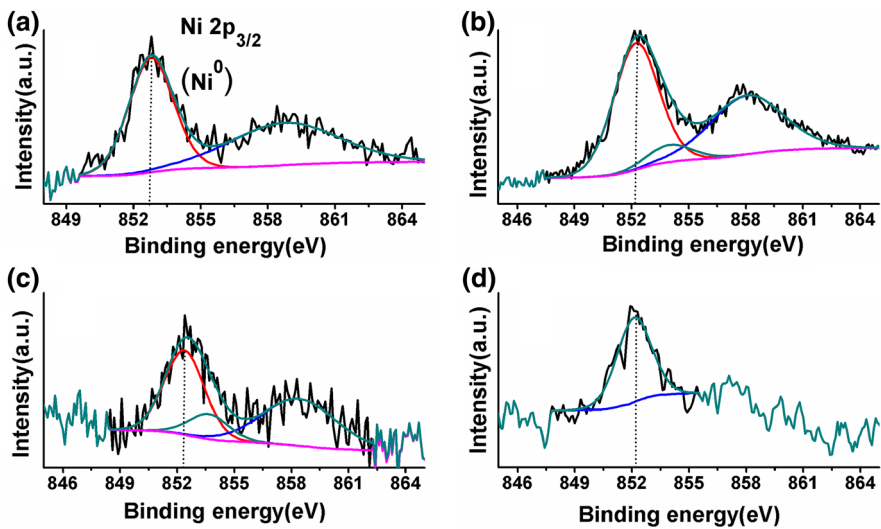


Fig. 5 XPS Profiles for Ni 2p level a Ni/TiO₂ b Co_{0.5} Ni_{0.5}/TiO₂ c Co_{0.6} Ni_{0.4}/TiO₂ d Co_{0.7} Ni_{0.3}/TiO₂

Table 2 XPS binding energy data for Co–Ni catalysts

Catalysts	Co 2p _{3/2} (eV)	Ni 2p _{3/2} (eV)
Co	778.4	–
Co _{0.7} Ni _{0.3}	778.8	852.2
Co _{0.6} Ni _{0.4}	778.9	852.3
Co _{0.5} Ni _{0.5}	778.7	852.3
Ni	–	852.8

BE value of 778.4 eV observed for Co2p_{3/2} energy level in monometallic Co/TiO₂ (Fig. 4a) indicates that Co is in metallic state and is in line with the values reported in the literature [22, 37]. Small amounts of Co in oxidized state, observed at higher BE, are due to surface oxidation by atmospheric oxygen during handling of the catalysts. Introduction of Ni results in the shifting of Co2p_{3/2} BE to the higher side, by 0.3–0.5 eV (Fig. 4b–d; Table 2). The shift in BE of metallic Co could be due to charge transfer from Co to Ni in the formation of alloys. Similarly, the BE value of 852.8 eV observed for Ni2p_{3/2} energy level in monometallic Ni/TiO₂ (Fig. 5a) indicates that Ni is in a metallic state and is also in line with the values reported in the literature [22, 38]. Again, small amounts of Ni in an oxidized state are observed, due to surface oxidation during handling of the catalysts. Shifts in BE values for the Ni2p_{3/2} level in bimetallic Co–Ni catalysts (Fig. 5b–d; Table 2) show a reverse trend compared to that observed for Co 2p_{3/2} level, a decrease of 0.5–0.6 eV with respect to that for monometallic Ni/TiO₂. Changes in BE values observed for both Co 2p_{3/2} and Ni2p_{3/2} are indicative of nanoscale Co–Ni alloy formation. XPS studies on bimetallic Co–Ni supported on anatase TiO₂ by Takanahe et al. [22] did not reveal changes in BE values, possibly due to the catalyst preparation method used (incipient wetness). Simultaneous chemical reduction of Co²⁺ and Ni²⁺, adopted in the present work, has resulted in more effective nanoscale interactions between Co and Ni. No significant changes in the surface composition of Co and Ni are observed. Corresponding to the bulk composition of Co_{0.5}Ni_{0.5}, the surface atomic composition of Co and Ni, calculated from XPS data, turns out to be 44% Co and 56% Ni. A slight surface enrichment of Ni could be due to the lower surface energy of Ni vis-a- vis that for Co [38].

H₂ temperature programmed desorption

H₂-TPD studies have been used to investigate the type and strength of active catalytic centers for hydrogen chemisorption. Figure 6 displays H₂-TPD profiles TiO₂ supported Co and Ni monometallic and six bimetallic catalysts. Distinct desorption peaks observed on all the catalysts indicate the presence of metal sites that bind hydrogen with varying strength. Peaks in the temperature range 100–200 °C are attributed to desorption from dispersed Co/Ni metal sites and those at higher temperatures, to desorption of spilled over hydrogen on support sites [39–41]. Monometallic Co displays desorption peak at 118 °C and Ni at 134 °C. With the addition of a 0.2 atomic fraction of Ni to Co (Co_{0.8}Ni_{0.2}), the low temperature H₂ TPD peak shifts to 112 °C. With further addition of Ni (Co_{0.7}Ni_{0.3} and Co_{0.6}Ni_{0.4}) desorption maxima is shifted to lower temperatures, 110 and 106 °C, respectively, indicating gradual weakening of M–H bond strength. With Co_{0.5}Ni_{0.5} and Co_{0.4}Ni_{0.6}, desorption maxima are again at lower temperatures, 121 and 112 °C, respectively. TPD maximum for Co_{0.2}Ni_{0.8} however is at 134 °C, similar to that observed for monometallic Ni/TiO₂. Thus for specific Co–Ni compositions, weakening of M–H bond strength, possibly due formation of Co–Ni alloys, is observed. Weaker M–H bonds may favour facile hydrogenation.

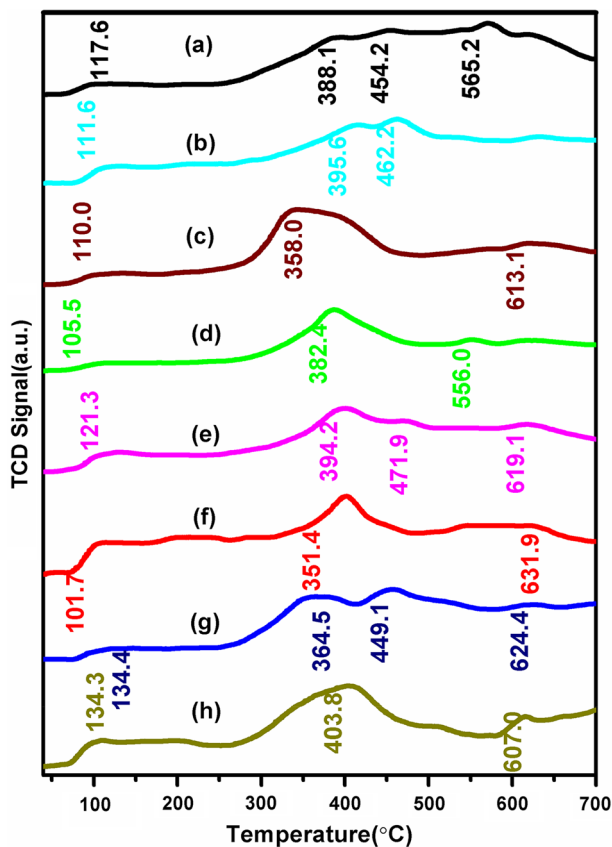


Fig. 6 H₂-TPD Profiles for *a* Co/TiO₂ *b* Co_{0.8}Ni_{0.2}/TiO₂ *c* Co_{0.7}Ni_{0.3}/TiO₂ *d* Co_{0.6}Ni_{0.4}/TiO₂ *e* Co_{0.5}Ni_{0.5}/TiO₂ *f* Co_{0.4}Ni_{0.6}/TiO₂ *g* Co_{0.2}Ni_{0.8}/TiO₂ *h* Ni₁/TiO₂

Hydrogenation of cinnamaldehyde

Table S2 gives CAL conversion and selectivity for different products, HCAL, COL and HCOL at different temperatures on mono- as well as bimetallic catalysts. Formation of acetals as a side product has been minimized (2.8% max) by using isopropanol and water mixture as solvent. CAL conversion and selectivity for various products at 140 °C on all catalysts are presented in Fig. 7.

Hydrogenation of cinnamaldehyde on monometallic Co and Ni catalysts

Activity and selectivity values for Co and Ni monometallic catalysts tabulated in Table S2 are in line with the reported data [16, 17, 42, 43]. Ni/TiO₂ displays very high conversion of CAL (86.9%) with high selectivity (78.7%) towards HCAL formation at 140 °C. Co/TiO₂, on the other hand, exhibits relatively lower CAL conversion (55%) and higher selectivity (61.3%) for COL formation at the same

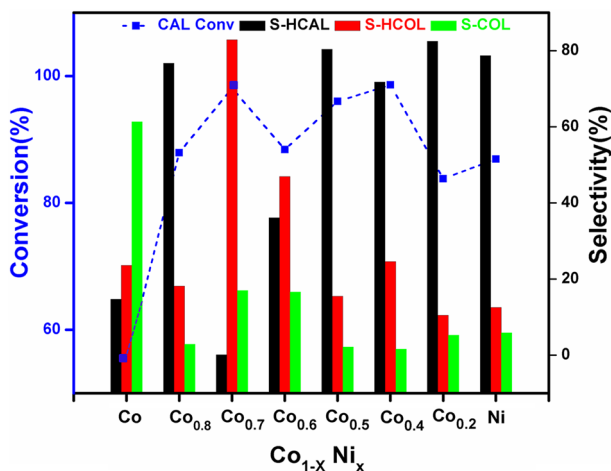


Fig. 7 CAL conversion and product selectivity values for Co–Ni catalysts. (Reaction conditions: 15 g isopropanol + 1.65 g water and 1.2 g CAL, Temp. 140 °C, Pressure 20 bar)

temperature. Similar trends for both catalysts are observed at other temperatures as well (Table S2).

Singh and Vannice [44] have observed volcano type correlation between % d-character (δ) of the metals and the initial TOF values for liquid phase hydrogenation of citral, a typical unsaturated aldehyde like cinnamaldehyde, on a series of silica supported Group VIII metal catalysts. The % d-character (δ), as described and calculated by Pauling [45], represents electronic structure of metals and gives a measure of the contribution of d-electrons to the hybrid spd orbitals of the metal. Correlations between δ values for Group VII metals and hydrogenation [46] and hydrogenolysis [47] activities have been reported. While Pd/SiO₂ with optimum % d character value displays maximum initial TOF, Co/SiO₂ with lowest % d-character value shows lowest activity. Ni/SiO₂, with relatively higher % d-character value with respect to Co/SiO₂, displays higher initial TOF [44].

In the present work, the difference in the activity of Ni and Co catalysts with TOF values of 1.69 and 1.08 h⁻¹ respectively, observed for hydrogenation on cinnamaldehyde (Table 1) could be explained on the basis of their % d-character values that influence the adsorption and activation of the unsaturated aldehydes.

According to Delbecq and Sautet [48], the selectivity for hydrogenation of C=O versus C=C is related to the width of the d-band [48, 49]. Os, Ir, Ru and Pt with higher d-band width exhibit higher selectivity towards C=O hydrogenation, while Pd, Rh and Ni with lower width, preferentially activate C=C for hydrogenation. Accordingly, Co with higher d-band width (4.0 eV) vis-à-vis Ni (3.0 eV) exhibits higher selectivity for C=O hydrogenation. However, it is pertinent to note that the concept of d-band width could explain the selectivity for C=O versus C=C hydrogenation in the case of 3d, 4d and 5d metals, but with some exceptions. Pd (4.1 eV) and Rh (4.4 eV) with d-band width closer to that for Co (4.0), display higher selectivity for C=C hydrogenation. Hence, d-band width alone could not be

the factor responsible for higher selectivity for C=O hydrogenation observed with Co.

Adsorption of CAL through C=O could be the primary route [42] for COL formation on Co catalysts. Of the five possible modes of adsorption of α , β -unsaturated aldehydes like CAL, proposed by Delbecq and Sautet [48], the three possible modes for C=O adsorption are, namely, on-top η_1 , di- σ η_2 and $\pi_{CO}\eta_2$ leading to the formation of COL. In the absence of experimental data on the mode of adsorption of CAL on the Co surface, on-top η_1 could be the likely mode, based on the in situ IR spectral data for adsorption of acetone on the Co surface [50] though adsorption in $\pi_{CO}\eta_2$ mode could not be ruled out. Adsorption of CAL on the Ni surface could be through $\pi_{C=C}$ η_2 or $\sigma_{C=C}$ η_2 , resulting in the formation of HCLA. Since hydrogenation of C=C is kinetically favored vis-à-vis that of C=O, conversion of CAL on Co is lower than that on Ni. This aspect is also reflected in experiments when neat HCAL or COL is used as feeds on Co (Table 3). While 33.8% of HCAL undergoes conversion on Co in 1 h, only 14.4% COL is converted during that period. The corresponding behavior is just the reverse on Ni, with 57.9% COL conversion and only 17.5% conversion of HCAL. It is clear that in the absence of conjugated C=C and C=O bonds, hydrogenation of C=C is preferred on Co while hydrogenation of C=O is facile on Ni. Similar trends are observed when mixtures of HCAL and COL and CAL and COL are used as feed (Table 3). Thus, competitive adsorption of products (HCAL and COL) on Co and Ni [42] also influences the reaction pathways and hence the selectivity.

Hydrogenation of cinnamaldehyde on bimetallic Co and Ni catalysts

Activity and selectivity data for Co–Ni bimetallic catalysts at different reaction temperatures are given in Table S2. Graphical representation of CAL conversion/selectivity data for Co–Ni series of catalysts at 140 °C are presented in Fig. 7 and discussed further. Under identical reaction conditions, substitution of a 0.2 atomic fraction of Co with Ni (Co_{0.8}Ni_{0.2}) results in significant improvement in CAL conversion (55–87.9%) vis-à-vis Co/TiO₂, accompanied by sharp decrease in selectivity for COL (61.3–2.9%) and increase in selectivity for HCAL (14.7–76.7%). On further substitution of Co by Ni to yield Co_{0.6}Ni_{0.4} composition,

Table 3 Influence of feedstock composition on conversion (%)

Feed stock composition					
Catalysts	100%CAL	100%HCAL	100%COL	50%HCAL + 50%COL	50%CAL + 50%COL
Co _{1.0}	26.1	33.8	14.4	40.7 + 25.4	62.5 + 5.8
Co _{0.7} Ni _{0.3}	84.0	99.1	63.4	97.6 + 56.6	98.0 + 3.6
Co _{0.6} Ni _{0.4}	51.4	78.0	47.9	69.8 + 31.8	88.5 + 90.6
Ni _{1.0}	62.1	17.5	57.9	21.3 + 30.9	55.8 + 73.9

Reaction conditions-(Reaction conditions-Reaction conditions: Temp-120 °C, 15 g isopropanol + 1.65 g water and 1.2 g CAL)

nearly the same CAL conversion (88.4%) is maintained, but significant changes on selectivity of products is observed. While the selectivity for HCAL decreases from 76.7% to 36.1%, selectivity for COL increases to 16.6% along with an increase in selectivity towards HCOL (46.9%), indicating further hydrogenation of COL to HCOL.

Bi-metallic catalyst with an intermediate composition, namely, Co_{0.7}Ni_{0.3}, exhibits interesting behavior, with high CAL conversion (98.1%), and selectivity to COL and HCOL at 17 and 82.9% respectively, indicating very high overall hydrogenation activity. TPR studies on this catalyst reveal increase in overall reducibility (Figs. 3, S2).

The catalyst with composition with relatively higher Ni content, Co_{0.5}Ni_{0.5}, maintains nearly same CAL conversion (96%), but selectivity for HCAL is a maximum at 80.4%, followed by 15.5% selectivity to HCOL and very low selectivity to COL (2.2%). With further increase in Ni, the catalyst Co_{0.4}Ni_{0.6}, high CAL conversion is maintained at 98.6% with HCAL (71.8%) and HCOL (24.6%) as major products. The catalyst with composition Co_{0.2}Ni_{0.8} displays CAL conversion and a product selectivity pattern which closely resemble those for monometallic Ni.

To summarize, at a constant reaction temperature of 140 °C, an exceptional increase in CAL conversion up to > 98% is observed in composition range $x = 0.3$ to 0.6. Maximum selectivity to HCOL (82.9%) is realized with Co_{0.7}Ni_{0.3}, while maximum selectivity to HCAL (80.4%) with Co_{0.5}Ni_{0.5}. While Co rich phases facilitate further hydrogenation of COL to HCOL, Ni rich phases exhibit high selectivity towards HCAL. Overall CAL hydrogenation activity at 140 °C, when expressed as TOF (Table 1), displays a maximum value at the composition Co_{0.5}Ni_{0.5}. Similar trends are observed at 120 and 130 °C as well.

In the present work, H₂-TPD studies (Fig. 6) have shown that, on Co_(1-x)Ni_x catalysts with x values in the range 0.3–0.6, the desorption of hydrogen from metal sites occurs at lower temperatures compared to that on monometallic Co or Ni. Thus, both Co–Ni alloy formation, as observed by TPR and XPS and weaker M–H bonds improve the CAL conversion, vis-à-vis monometallic Co and Ni. Weaker M–H bonds, especially in Co_{0.7}Ni_{0.3} and Co_{0.6}Ni_{0.4}, facilitate further hydrogenation of COL to HCOL. On these catalysts, higher selectivity to COL (42.8 and 25.9%, respectively) could be achieved at lower reaction temperature, 120 °C (Table S2).

Relevance of alloy formation in achieving higher CAL conversion is further supported by carrying out CAL conversion on mechanical mixture of separately pre-reduced Co/TiO₂ and Ni/TiO₂. Mechanical mixture of pre-reduced component catalysts, corresponding to the composition Co_{0.7}Ni_{0.3} at 140 °C, showed CAL conversion of 32.6% with selectivity to HCAL, HCOL, COL and ACTL being 68.6, 15.8, 10.5 and 5.0%, respectively, compared to the very high CAL conversion of 98.1% on Co_{0.7}Ni_{0.3} prepared by simultaneous reduction of the metal acetates by glucose, wherein alloy formation is facilitated.

As observed in the TPR and XPS measurements, Co–Ni alloy formation in the composition range $x = 0.3$ –0.6 enhances overall reducibility by controlling the degree of interaction of the metals with the support. Alloying also shifts the d-band centre, thus modifying the electronic character and influencing the nature of adsorption of the reactants [51].

Availability of active hydrogen with weaker M–H bond strength is known [26–36] to increase the activity for hydrogenation, facilitating the hydrogenation of coke precursors in steam reforming of methane and dry reforming with CO₂. Such a synergetic effect between Co- & Ni resulting in improved reducibility, dispersion and alloy formation is responsible for the high activity of Co–Ni bimetallic catalysts for hydro de-oxygenation (HDO) of bio-oils [52] and hydrogen production by decomposition of cellulose and glycerol [53, 54]. Base metal catalysts with appropriate composition of Co and Ni emerge as highly effective catalysts for different hydrogenation and hydrogenolysis reactions and economically viable alternatives to noble metal based catalysts.

It is pertinent to mention at this stage that Malobela et al. [15] could achieve COL selectivity of 62% on Co–Ni (5% w/w each) catalyst at lower CAL conversion (63%) on MWCNT support, which does not facilitate adsorption of CAL via the C=C bond, due to the increase in electron density around Co/Ni.

In contrast to this work, Hui et al. [14] in their studies on ternary system Ni–Co–B observed a moderate increase in activity (64.6% maximum) for CAL hydrogenation over a broad composition of (Co/Co + Ni) ranging from 0.2 to 0.5 and no change on selectivity to HCAL. H₂-TPD studies by Hui et al. [14] showed that on Co–B desorption of hydrogen occurs at a lower temperature compared to that on Ni–B indicating that the presence of Co with Ni could lead to weaker M–H bonds, resulting in higher activity, which is in line with the observations in the present work

Recycling and stability of the bimetallic catalyst

The used catalyst (Co_{0.3}Ni_{0.7}) after 1 h reaction time is separated and washed with iso-propyl alcohol several times and hydrogenation of CAL is carried out again. The catalyst displays nearly the same conversion and selectivity as that of the fresh catalyst for four such cycles (Table S3). ICP-OES data (Table S1) shows that the metal composition is intact with no leaching. No significant change in the crystallite size of Co/Ni is observed on the TE micrograph (Fig. 2i) for the used catalyst, indicating the stability of the catalyst under reaction conditions.

Conclusions

Selective hydrogenation of cinnamaldehyde has been investigated on a series of bi-metallic Co–Ni catalysts in the composition range Co_(1-x)Ni_x with $x = 0.0, 0.2, 0.3, 0.4, 0.5, 0.6, 0.8$ and 1.0, with total metal loading of 15% w/w and supported on TiO₂-P25. TPR and XPS results indicate the formation of nanoscale Co–Ni alloys and increase in reducibility of Co and Ni in the composition range $x = 0.3–0.6$, besides weakening of M–H bond strength, as revealed by H₂-TPD measurements. Unlike the monometallic Co and Ni catalysts, bi-metallic Co–Ni catalysts in the composition range $x = 0.3–0.6$ display very high conversion (> 98%) of cinnamaldehyde (CAL). Bimetallic Co_{0.7}Ni_{0.3} catalyst displays high conversion of CAL (98.1%) and high selectivity (82.9%) towards hydrocinnamyl alcohol

(HCOL). Overall CAL hydrogenation activity at 140 °C, when expressed as TOF, displays a maximum value at the composition Co_{0.5}Ni_{0.5}. Co–Ni alloy formation, which modifies the electronic structure, d-band characteristics and M–H bond strength, is responsible for the observed changes in activity and selectivity. The catalysts display stable activity and selectivity for four cycles and no changes in the metal composition or metal crystallite size are observed after use. A synergetic effect, originating from an appropriate composition of Co and Ni and reaction conditions, results in highly effective and economically viable base metal catalysts for hydrogenation reactions, in comparison with noble metal based catalysts.

Acknowledgements The authors are thankful to the Department of Science and Technology, Govt. of India, for establishing the research facilities at the National Centre for Catalysis Research for carrying out this work and IIT Madras for providing infrastructure support.

Compliance with ethical standards

Conflict of interest The authors declared that they have no conflict of interest.

References

1. P. Gallezot, D. Richard, *Catal. Rev. Sci. Eng.* **40**, 81 (1998)
2. A. Giroir-Fendler, D. Richard, P. Gallezot, in *Studies in Surface Science and Catalysis*, vol. 41, ed. by J. Barrault, C. Bouchoule, D. Duprez, C. Montassier, M. Guisnet, G. Pérot (Elsevier, Amsterdam, 1988), pp. 171–178
3. M.G. Prakash, R. Mahalakshmy, K.R. Krishnamurthy, B. Viswanathan, *Catal. Today* **263**, 105 (2016)
4. W. Yu, Y. Wang, H. Liu, W. Zheng, *J. Mol. Catal. A* **112**, 105 (1996)
5. B. Coq, P.S. Kumbhar, C. Moreau, P. Moreau, M.G. Warawdekar, *J. Mol. Catal.* **85**, 215 (1993)
6. B. Coq, P.S. Kumbhar, C. Moreau, P. Moreau, F. Figueras, *J. Phys. Chem.* **98**, 10180 (1994)
7. R. Basale, Ph.D. Thesis, (Tech. Univ. Eindhoven, Netherland, 2013)
8. P. Mäki-Arvela, L.P. Tiainen, M. Lindblad, K. Demirkan, N. Kumar, R. Sjöholm, T. Ollonqvist, J. VäyrynenSalmi, DYu. Murzin, *Appl. Catal. A* **241**, 271 (2003)
9. X. Yuan, J. Zheng, Q. Zhang, S. Li, Y. Yang, *J. Gong, AIChE J.* **60**, 1036 (2012)
10. E. Asedegbega-Nieto, B. Bachiller-Baeza, A. Guerrero-Ruiz, I. Rodriguez-Ramos, *Appl. Catal. A* **300**, 120 (2006)
11. H. Noller, W.M. Lint, *J. Catal.* **85**, 25 (1984)
12. S.A. Ananthan, V. Narayanan, *Int. J. Chem.* **3**, 55 (2011)
13. B.M. Reddy, G.M. Kumar, I. Ganesh, A. Khan, *J. Mol. Catal. A: Chem.* **247**, 80 (2006)
14. L.I. Hui, M.A. Chun-Jing, L.I. He-Xing, *Acta Chim. Sinica* **64**, 1947 (2006)
15. L.J. Malobela, J. Heveling, W.G. Augustyn, L.M. Cele, *Ind. Eng. Chem. Res.* **53**, 13910 (2014)
16. W. Lin, H. Chang, L. He, Y. Yu, F. Zhang, *J. Catal.* **303**, 110 (2013)
17. K.J.A. Raj, M.G. Prakash, T. Elangovan, B. Viswanathan, *Catal. Lett.* **142**, 87 (2011)
18. M. Vasseem, N. Tripathy, G. Khang, Y. Halm, *RSC. Adv.* **3**, 9698 (2013)
19. H.B. Boubaker, M. Mhamdi, E. Marceau, S. Khaddar-Zine, A. Ghorbel, M. Che, Y.B. Taarit, F. Villain, *Microporous Mesoporous Mater.* **93**, 62 (2006)
20. R. Li, X. Ren, H. Ma, X. Feng, Z. Lin, X. Li, C. Hu, B. Wang, *J. Mater. Chem. A* **2**, 5724 (2014)
21. R.J. Isaifan, H.A.E. Dole, E. Obeid, L. Lizarraga, P. Vernoux, E.A. Baranova, *Electrochem. Solid-State Lett.* **15**, E14 (2012)
22. K. Takanabe, K. Nagaoka, K. Nariai, K. Aika, *J. Catal.* **232**, 268 (2005)
23. M.M. Van Schooneveld, C. Campos-Cuerva, J. Pet, J.D. Meeldijk, J. van Rijssel, A. Meijerink, B.H. Erne, F.M.F. de Groot, *J. Nanopart. Res.* **14**, 991 (2012)
24. X.B. Zhang, Y.J. Zhang, F. Chen, Y.Z. Xiang, B. Zhang, L.Y. Xu, T.R. Zhang, *Reac. Kinet. Mech. Cat.* **115**, 283 (2015)

25. D. Golodnitsky, N.V. Gudim, G.A. Volyanuk, J. Electrochem. Soc. **147**(11), 4156 (2000)
26. X. You, X. Wang, Y. Ma, J. Liu, W. Liu, X. Xu, H. Peng, C. Li, W. Zhou, P. Yuan, X. Chen, Chem. Cat. Chem. **6**, 3377 (2014)
27. M. Phongaksorn, S. Tungkamani, N. Dharmasaroja, T. Chamni, R. Chuvareec, N. Kanjanabat, N. Siri-Nguanc, Chem. Eng. Trans. **43**, 925 (2015)
28. X. Hu, G.X. Lu, J. Mol. Catal. A **261**, 43 (2007)
29. L.W. Chen, C.K.S. Choong, Z.Y. Zhong, L. Huang, Z. Wang, J.Y. Lin, Int. J. Hydrog Energy **37**, 16321 (2012)
30. H. Woo, R. Srinivasan, L. Rice, R. De Angelis, P. Reucroft, J. Mol. Catal. **59**, 83 (1990)
31. I. Tatsumi, E. Koichi, A. Hiromichi, Appl. Catal. **30**, 225 (1987)
32. P.C. Das, N.C. Pradhan, A.K. Dalai, N.N. Bakshi, Catal. Lett. **98**, 153 (2004)
33. H. Luo, H. Li, H.L. Zhuang, Chem. Lett. **5**, 404 (2001)
34. L. Wei, C. Xianian, L. Jin, Y. Ying, Z. Yongfu, H. Zhaolong, Y. Zhengzhou, Adv. Malts. Res. **430**, 917 (2012)
35. W. Lin, H. Chang, L. He, Y. Yu, F. Zhang, J. Catal. **303**, 110 (2013)
36. D. Xu, W. Li, H. Duan, Q. Ge, H. Xu, Catal. Lett. **102**, 229 (2005)
37. N.S. McIntyre, M.G. Cook, Anal. Chem. **47**, 2208 (1975)
38. H.L. Skriver, N.M. Rosengaard, Phys. Rev. B **46**, 7157 (1992)
39. S. Velu, S. Gangwal, Solid State Ion. **177**, 803 (2006)
40. A.G. Boudjahem, S. Monteverdi, M. Mercy, D. Ghanbaja, M.M. Bettahar, Catal. Lett. **84**, 115 (2002)
41. J. Liu, C. Li, F. Wang, S. He, H. Chen, Y. Zhao, M. Wei, D.G. Evans, X. Duan, Catal. Sci. Technol. **3**, 2627 (2013)
42. Y. Nitta, K. Ueno, T. Imanaka, Appl. Catal. **56**, 9 (1989)
43. C. Rudof, B. Dragoi, A. Ungureanu, A. Chiriac, S. Royer, A. Nastroc, E. Dumitriu, Catal. Sci. Technol. **4**, 179 (2014)
44. U.K. Singh, M.A. Vannice, J. Catal. **199**, 73 (2001)
45. L. Pauling, Proc. R. Soc. A **196**, 343 (1949)
46. O. Beeck, Faraday. Soc. Discuss. **8**, 118 (1950)
47. J.H. Sinfelt, Science **195**, 641 (1977)
48. F. Delbecq, P. Sautet, J. Catal. **152**, 217 (1995)
49. C.S. Fadley, D.A. Shirley, 3rd materials research symposium—electronic density of states. Nov. 3–6, 1969, Gaithersburg, MD
50. G. Blyholder, D. Shihabi, J. Catal. **46**, 91 (1977)
51. T. Bligaard, J.K. Nørskov, in *Chemical Bonding at Surfaces and Interfaces*, 1st Edn., ed. by A. Nilsson, L.G.M. Pettersson, J.K. Nørskov (Elsevier, Amsterdam, 2008)
52. T.M. Huynh, U. Armbruster, L.H. Nguyen, D.A. Nguyen, A. Martin, J. Sustain. Bioenergy Syst. **5**, 151 (2015)
53. M. Zhao, T.L. Church, A.T. Harris, Appl. Catal. B **101**, 522 (2011)
54. Y. Wang, M. Chen, Z. Yang, T. Liang, S. Liu, Z. Zhou, X. Li, Appl. Catal. A. Gen. **550**, 214 (2018)

Affiliations

Saranya Ashokkumar^{1,2} · Vivekanandan Ganesan² ·
Krishnamurthy K. Ramaswamy¹ · Viswanathan Balasubramanian¹

✉ Viswanathan Balasubramanian
bviswanathan@gmail.com

¹ National Centre for Catalysis Research (NCCR), Indian Institute of Technology, Madras, Chennai 600036, India

² Department of Chemistry, A V C College, Mayiladuthurai 609305, India